Int. J. Heat Mass Transfer. Vol. 31, No. 6, pp. 1269–1278, 1988
Printed in Great Britain

0017–9310/88 $3.00 + 0.00

The dynamic characteristics of a countercurrent plate heat exchanger

A. R. KHAN, N. S. BAKER and A. P. WARDLE
Department of Chemical Engineering, University College of Swansea, Singleton Park, Swansea SA2 8PP, U.K.

(*Received* 28 *October* 1986 *and in final form* 20 *November* 1987)

Abstract—Theoretical and experimental analyses of the dynamic characteristics of a plate heat exchanger have been carried out. First- and second-order models with dead time are proposed and checked against results obtained by experimental sinusoidal and pulse testing. It has been found that the dynamic response of the outlet temperature θ_{co} of the cold stream to variations in the mass flow m_h of the hot stream most closely approaches the second-order transfer function

$$\frac{\bar{\theta}_{co}(s)}{\bar{m}_h(s)} = \frac{H(\tau_a s+1)\,e^{-\tau_d s}}{\tau_p^2 s^2 + 2\zeta\tau_p s + 1}.$$

1. INTRODUCTION

THE DYNAMIC characteristics of shell and tube heat exchangers have been the subject of considerable study and numerous papers [1]. Plate heat exchangers (PHE) have received much less attention. However, the latter are of increasing importance due to their application in the chemical and petrochemical industries [2].

Over the last three decades several workers have published papers concerning the dynamic characteristics of different types of PHE in terms of the system response to changes in inlet flow and temperature. McKnight and Worley [3] demonstrated the application of feedback control related to high velocity flow in a PHE whilst Ito and Masubuchi [4] investigated the dynamics of PHE systems both theoretically and experimentally using three different types of fluid flow pattern. Zaleski and Tejszerski [5] developed a mathematical model to simulate the transient operation of two-fluid, multichannel PHEs with parallel flow arrangements.

No work appears to have been reported yet concerning the dynamics of a countercurrent flow PHE. The present investigation attempts to meet that need and consists of an experimental study of the unsteady-state behaviour of such an exchanger together with an appropriate theoretical analysis. Two experimental procedures have been employed using a 21-plate countercurrent flow PHE with water on both sides of the plates—one being the well-known frequency response approach whilst the other consists of a pulse technique with an analysis based upon the method of moments [6].

2. EXPERIMENTAL WORK AND COMPUTATION

The experimental rig and details of the design of the PHE employed in this work are presented in Figs. 1 and 2, respectively. The relevant steady-state parameters are listed in Table 1.

2.1. *Frequency response testing*

In this case a sinusoidal disturbance was imposed upon the flow of the hot stream entering the PHE by means of a signal generator connected to a pneumatic control valve (Fig. 1). The response of the temperature of the cold stream leaving the exchanger (θ_{co}) was recorded at 4 s intervals and the experimental programme was designed to cover a frequency range between 0.0063 and 0.44 rad s^{-1}. All temperatures were measured by means of chromel–alumel thermocouples.

The response of θ_{co} to the sinusoidal disturbance in hot stream flow rate may be represented by

$$\theta_{co}(t) = \theta_{co} + A\sin(\omega t + \phi) \tag{1}$$

where A is the amplitude of the output disturbance, ω the radian frequency of the applied disturbance, ϕ the phase shift between input and output, and θ the steady-state cold stream outlet temperature.

Values of θ_{co}, A and ϕ giving the best fit of equation (1) to the experimentally measured cold stream outlet temperature θ_j were obtained by a least squares procedure in which the sum of squares of the errors was expressed as

$$\text{S.S.E.} = \sum_{j=1}^{n} \{\theta_j - [\theta_{co} + A\sin(\omega t_j + \phi)]\}^2 \tag{2}$$

where n is the total number of observations.

Differentiating equation (2) with respect to θ_{co}, A and ϕ, respectively, and equating to zero leads to:

$$\theta_{co} = \frac{\sum_{j=1}^{n}\theta_j - A\sum_{j=1}^{n}\sin(\omega t_j + \phi)}{n} \tag{3}$$

NOMENCLATURE

A	heat transfer area [m^2]	θ	temperature [°C]
C	specific heat [J kg^{-1} °C^{-1}]	ϕ	phase lag [deg]
H	steady-state gain	τ	time constant [s]
K_1, K_2, etc.	constants defined in Appendices A and B	ω	frequency [rad s^{-1}].
M	hold-up mass [kg]		
m	mass flow rate [kg s^{-1}]		
n	number of experimental points		
s	Laplace operator	Subscripts	
t	time coordinate [s]	a	lead
U	overall heat transfer coefficient [W m^{-2} °C^{-1}]	c	cold
		d	dead
x	space coordinate [m].	h	hot
		i	inlet
Greek symbols		o	outlet
ζ	damping coefficient	p	process.

N.B. (a) quantities expressed as, e.g. $\theta_{co}(t)$ are considered to vary with time whereas those expressed as, e.g. θ_{co} are steady-state values;
(b) quantities expressed as, e.g. $\bar{\theta}_{co}$ represent deviation variables, i.e. $\bar{\theta}_{co} = \theta_{co}(t) - \theta_{co}$;
(c) quantities expressed as, e.g. $\bar{\theta}_{co}(s)$ represent the Laplace transforms of the appropriate (deviation) variables.

$$A = \frac{n\sum_{j=1}^{n}\theta_j\cos(\omega t_j+\phi) - \sum_{j=1}^{n}\theta_j\sum_{j=1}^{n}\cos(\omega t_j+\phi)}{n\sum_{j=1}^{n}\sin(\omega t_j+\phi)\cos(\omega t_j+\phi) - \sum_{j=1}^{n}\sin(\omega t_j+\phi)\sum_{j=1}^{n}\cos(\omega t_j+\phi)}$$

$$= \frac{n\sum_{j=1}^{n}\theta_j\sin(\omega t_j+\phi) - \sum_{j=1}^{n}\theta_j\sum_{j=1}^{n}\sin(\omega t_j+\phi)}{n\sum_{j=1}^{n}\sin^2(\omega t_j+\phi) - \left(\sum_{j=1}^{n}\sin(\omega t_j+\phi)\right)^2}. \quad (4)$$

Equation (4) is nonlinear and cannot be solved explicitly for ϕ, consequently an open-ended linear search technique was employed to determine ϕ from this. From the latter estimate of ϕ corresponding values of θ_{co} and A were determined from equations (3) and (4), respectively. Typical experimental results are presented in Fig. 3 together with the fitted sine wave (equation (1)) using values of θ_{co}, A and ϕ calculated from equations (3) and (4). The calculations were repeated for all the frequencies employed in the experimental programme (Table 2). The resulting amplitude ratio (A.R.) and phase shift are presented as functions of frequency in the form of a Bode diagram (Fig. 4).

Table 1

Stream	Flow rate (kg s^{-1})	Inlet temperature (°C)	Outlet temperature (°C)
Cold	0.233	32	46.3
Hot	0.24	72.8	58.1

Plate dimensions: length, 0.33 m; breadth, 0.1 m; heat transfer area/plate, 0.033 m^2; clearance between two plates, 2.57 mm.

2.2. *Pulse testing*

Rectangular pulses of differing amplitudes were introduced into the inlet flow of the hot stream via the pneumatic control valve. The outlet temperature of the cold stream was recorded again at 4 s intervals. A typical pulse disturbance and the corresponding response of θ_{co} are shown in Fig. 5. The area under the output disturbance was calculated in each case by numerical integration. From a comparison of this with the relevant input pulse were determined values of A.R. and phase shift by the method of moments. (The latter consists essentially of writing the Laplace transform of the distribution function as a power series in which the coefficients are proportional to the moments of the distribution. These coefficients are derived from the area under the output pulse and provide the corresponding values of A.R. and phase shift as functions of frequency [6].) A typical Bode diagram for a pulse disturbance is presented in Fig. 6.

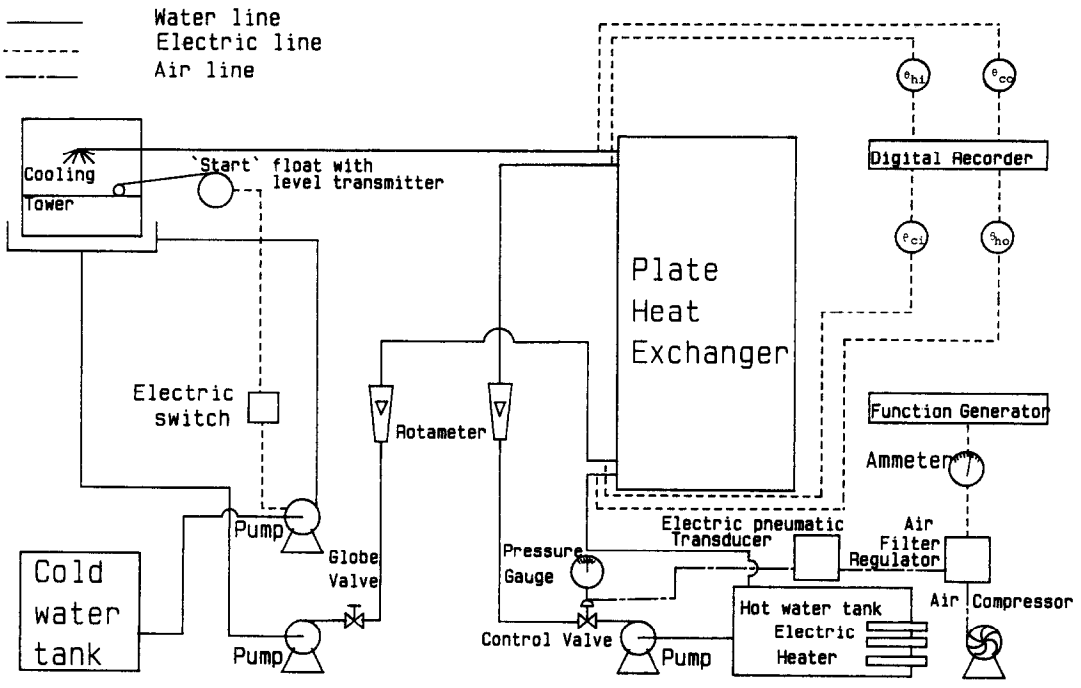

FIG. 1. Schematic diagram of plate heat exchanger rig.

3. THEORETICAL ANALYSIS

The following assumptions are frequently made in the modelling of plate heat exchangers [4, 7]:

(a) that heat losses to the surroundings are negligible and the two end plates of the exchanger serve as adiabatic walls;

(b) that heat transfer within the fluid in any channel is by convection only;

(c) that the fluid will split equally between the parallel channels for each stream;

(d) that the thermal capacity of the plate wall is negligible;

(e) that the temperature distributions in all channels belonging to the same stream are identical;

(f) that the film coefficient for heat transfer is dependent principally upon the fluid velocity and is proportional to an exponential function of the flow rate;

(g) that the physical properties of the fluid are constant over the range of temperatures employed.

These assumptions are incorporated in the development of a lumped parameter model in which the system may be described by unsteady-state energy balances across any specific plate as indicated in Fig. 2. Two approaches are possible. The first is to employ overall balances which assume that the overall heat transfer coefficient (U) is constant and the second is to consider that U is a function of the hot stream mass flow rate $m_h(t)$ which in turn is a function of time. Hence in the latter instance U is also a function of time, i.e. $U(t)$.

For U constant, a balance over the cold stream gives

$$m_c C(\theta_{ci}-\theta_{co}(t))+m_h(t)C(\theta_{hi}-\theta_{ho}(t)) = M_c C\frac{d\theta_{co}(t)}{dt} \tag{5}$$

and over the hot stream

$$m_h(t)C(\theta_{hi}-\theta_{ho}(t))+m_c C(\theta_{ci}-\theta_{co}(t)) = M_h C\frac{d\theta_{ho}(t)}{dt} \tag{6}$$

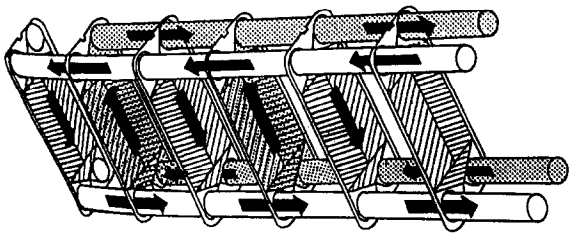

FIG. 2. Direction of flow in plate heat exchanger.

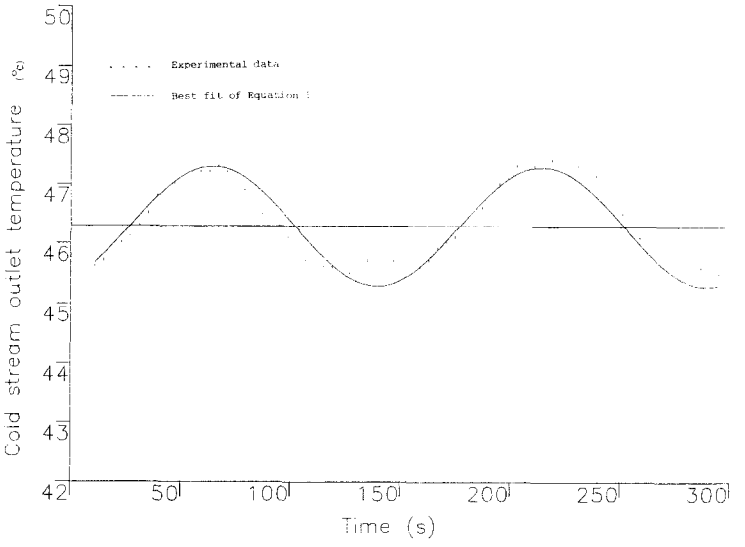

FIG. 3. Experimental response to sinusoidal disturbance.

($m_h(t)$, etc. represent quantities varying with time and all other are steady-state values and/or are assumed constant).

By linearizing non-linear terms, the introduction of deviation variables and the application of the Laplace transform, equations (5) and (6) may be simplified and solved simultaneously (Appendix A) to give the transfer function

$$G(s) = \frac{\bar{\theta}_{co}(s)}{\bar{m}_h(s)} = \frac{H}{1+\tau_p s} \tag{7}$$

which relates the outlet temperature of the cold stream (the controlled variable) to the mass flow rate of the hot stream (the manipulated variable).

Hence, in this instance $G(s)$ represents a first-order lag with steady-state gain H and time constant τ_p.

If U is a function of time then an energy balance over the cold stream gives

$$AU(t)\left\{\frac{\theta_{hi}-\theta_{co}(t)}{2}+\frac{\theta_{ho}(t)-\theta_{ci}}{2}\right\} - m_c C(\theta_{co}(t)-\theta_{ci}) = M_c C\frac{d\theta_{co}(t)}{dt} \tag{8}$$

and for the hot stream

$$m_h(t)C(\theta_{hi}-\theta_{ho}(t)) - AU(t)\left\{\frac{\theta_{hi}-\theta_{co}(t)}{2}+\frac{\theta_{ho}(t)-\theta_{ci}}{2}\right\} = M_h C\frac{d\theta_{ho}(t)}{dt}. \tag{9}$$

In equations (8) and (9) it is assumed that the temperature differences $(\theta_{hi}-\theta_{co}(t))$ and $(\theta_{ho}(t)-\theta_{ci})$ are sufficiently close to each other to allow an arithmetic mean temperature difference to be employed rather than the more accurate log mean temperature difference. $U(t)$ is related to $m_h(t)$ by [8]

Table 2. The calculated phase lag and gain for experimental and theoretical data

Frequency (rad s^{-1})	Experimental results from frequency response method (M_{hs} = 0.233 kg s^{-1}) Phase lag (deg)	Gain	Experimental results from method of moments (pulse input) (M_{hs} = 0.1875 kg s^{-1}) Phase lag (deg)	Gain
0.0063	21.318	1	4.49	1
0.025	25.41	0.691	17.81	0.997
0.044	43.23	0.612	31.33	0.992
0.063	65.83	0.557	44.83	0.984
0.123	74.1	0.523	87.30	0.923
0.183	102.4	0.414	132.6	0.873
0.250	109.1	0.416	175.0	0.793
0.314	145.2	0.270	217.6	0.707
0.377	163.6	0.220	258.2	0.633
0.440	179.5	0.150	297.5	0.577
0.503	183.8	0.134	336.2	0.559
0.563	196.37	0.067	373.5	0.496
0.630	203.1	0.06	418.6	0.469

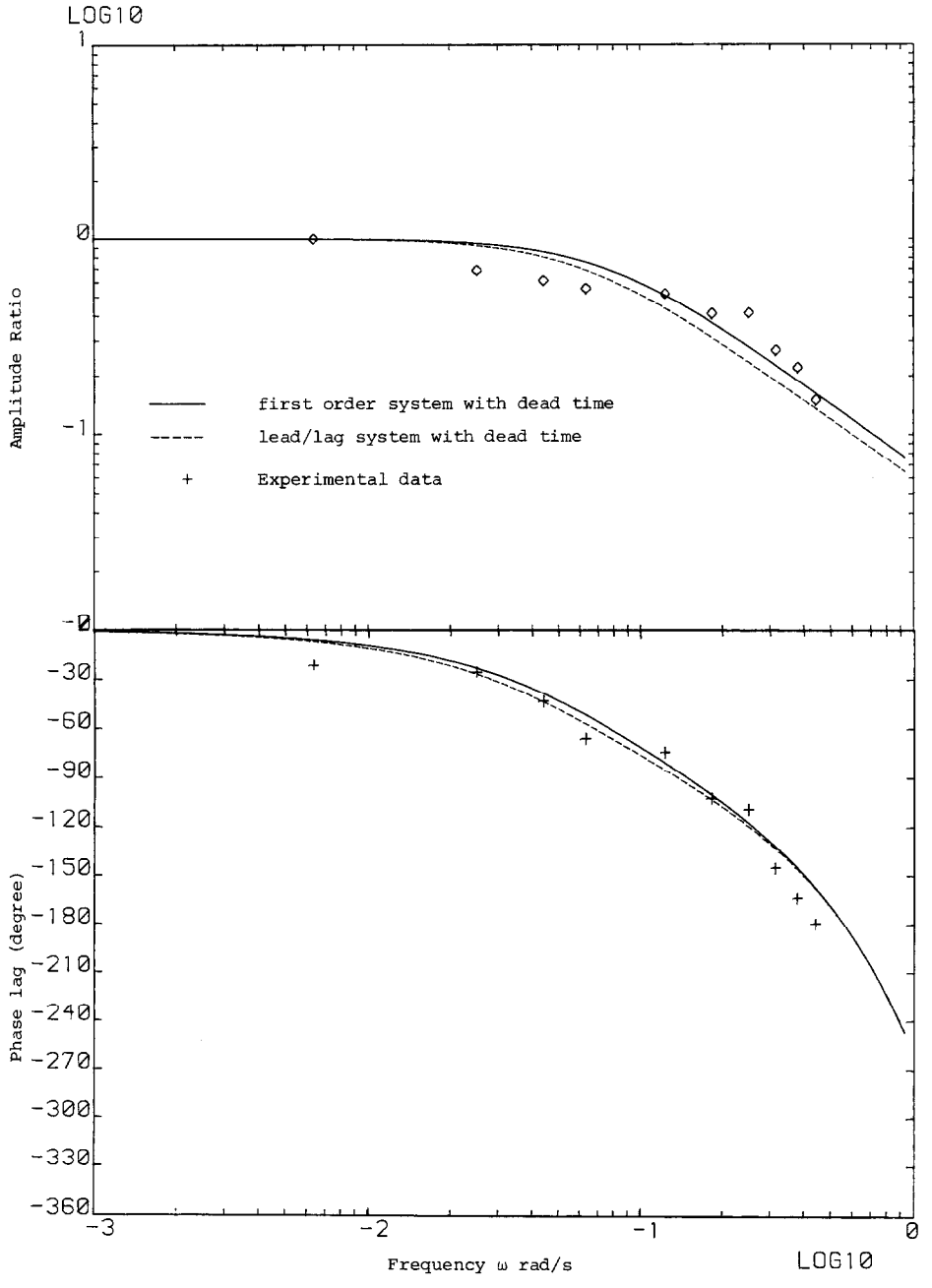

FIG. 4. Bode diagram for experimental data using sinusoidal disturbance.

$$\frac{1}{U(t)} = a + \frac{c}{[m_h(t)]^b}. \tag{10a}$$

The constants a, b and c have been evaluated from experimental data presented elsewhere [9], namely

$$\frac{1}{U(t)} = 1.2\times 10^{-3} + \frac{7.06\times 10^{-5}}{[m_h(t)]^{0.95}}. \tag{10b}$$

By substituting equation (10a) into equations (8) and (9), introducing deviation variables, applying the Laplace transformation and solving simultaneously (Appendix B)

$$G(s) = \frac{\bar{\theta}_{co}(s)}{\bar{m}_h(s)} = \frac{H(\tau_a s+1)}{\tau_p^2 s^2 + 2\zeta\tau_p s + 1}. \tag{11}$$

Thus if U is considered to be a function of t then the resulting transfer function $G(s)$ between θ_{co} and m_h consists of a second-order lag with time constant τ_p and damping coefficient ζ combined with a first-order lead element having a time constant τ_a.

4. RESULTS AND DISCUSSION

It is necessary to determine whether the PHE system in practice approaches either of the two models pro-

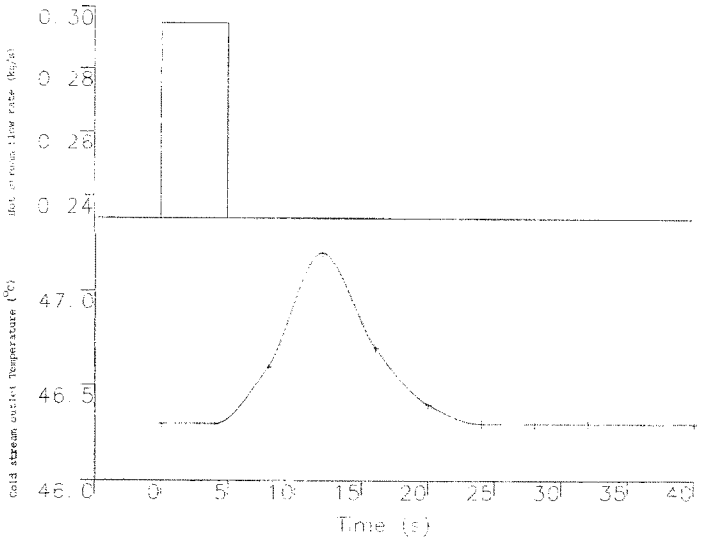

FIG. 5. Input pulse and response.

posed above. However, both are unrealistic insofar as they do not include any dead time. This must be present in any temperature system. The experimental results in Figs. 4 and 5 indicate phase lags in excess of 90° and 180° which would be the maximum attainable with a simple first- or second-order system, respectively. The additional lags exhibited are more likely to be due to the presence of dead time rather than to a higher order model. Hence, assuming that the PHE may be described by a first-order lag with dead time τ_d the relevant time constants were determined from the experimental results using an optimization procedure with an objective function of the form

$$F = \sum_{j=1}^{n} [\phi_j - \tan^{-1}(\omega_j \tau_p) - \omega_j \tau_d]^2. \quad (12)$$

Values of τ_p and τ_d were calculated for minimum F by the use of a multivariable non-linear approach which is a modified form of Rosenbrock's optimization method [10]. For the second-order lag/first-order lead model with dead time, the appropriate objective function becomes

$$F = \sum_{j=1}^{n} \left[\phi_j - \tan^{-1} \frac{-2\zeta\omega_j\tau_p}{1-\omega_j^2\tau_p^2} + \tan^{-1}\omega_j\tau_a - \omega_j\tau_d \right]^2. \quad (13)$$

The time constants in equation (13) for minimum F were determined with the same non-linear optimization technique. Values of ϕ_j employed in equations (12) and (13) were the experimental phase shifts obtained firstly using the sinusoidal forcing function and secondly employing the pulse technique. Time constants calculated for each type of model and each type of disturbance are listed in Table 3. A measure of the fit of each model to the experimental results is given by the respective correlation coefficient. It can be seen that the latter is much closer to unity for the lead/lag system with dead time than for the first-order system. This indicates that the lead/lag model fits the experimental data better for both sinusoidal and pulse disturbances. This agrees with the results of Burns *et al.* [11] who suggested such a system for modelling thermal regeneration systems and Gilles [12] who

Table 3. Transfer function parameters for first-order system and lead/lag system with dead time

	First-order system with dead time		Lead/lag system with dead time			
	Process time constant	Dead time	Lag time constant	Damping ratio	Lead time constant	Dead time
1. Experimental results for frequency response method	16.6	3	4.63	1.64	1.51	3
2. Experimental results of method of moments	2.5	10	3.6	1.1	5.4	10
	range of correlation coefficient for this case is 0.92–0.97		range of correlation coefficient for this case is 0.98–0.997			

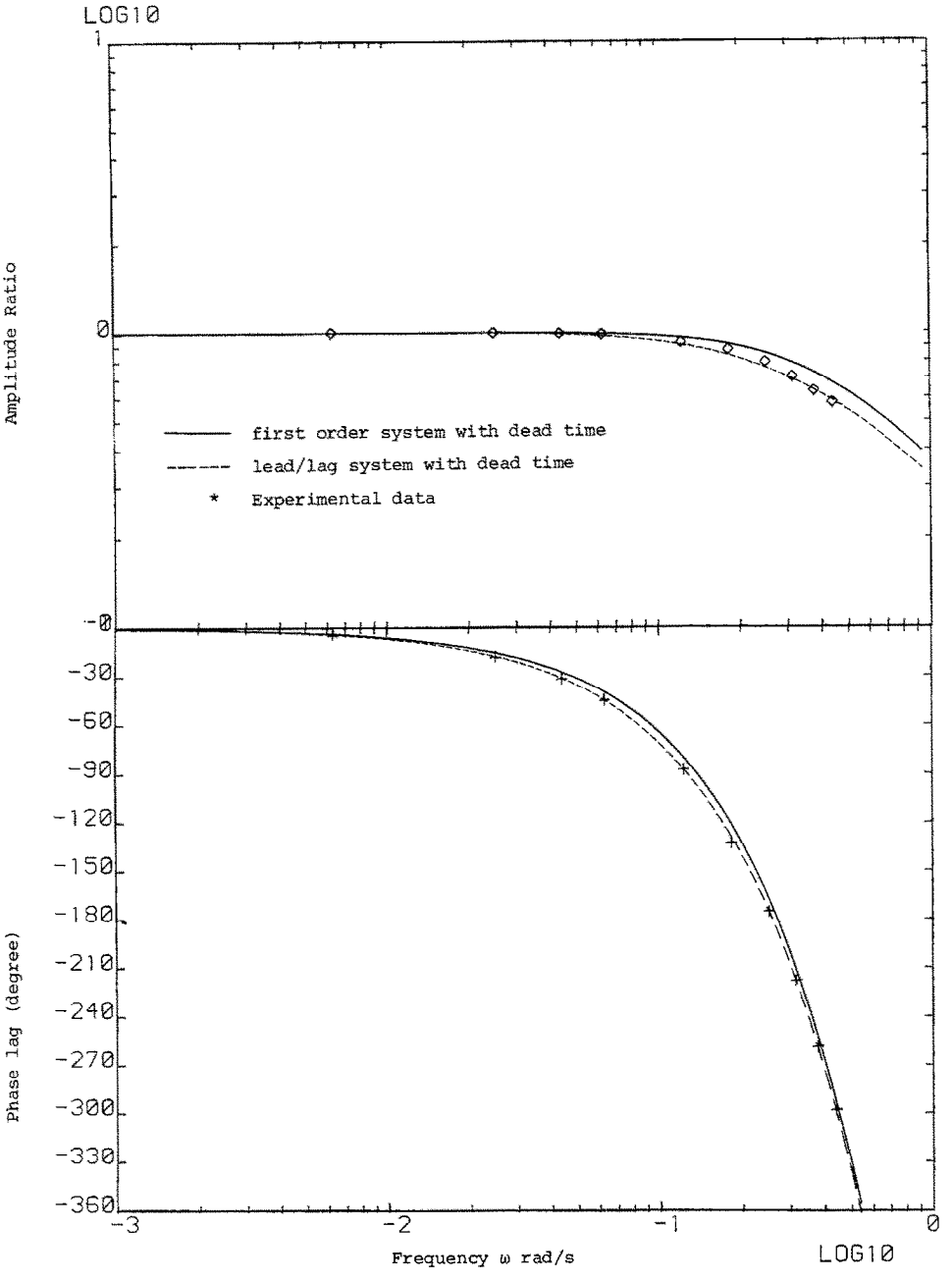

FIG. 6. Bode diagram for experimental data using method of moments.

compared a theoretical model of a countercurrent tubular heat exchanger with experimental results.

Examination of Fig. 4 reveals greater discrepancies in the case of the sinusoidal disturbances between the frequency response results at certain frequencies for the models and for the experimental results than obtained with the pulse changes. This is because in the case of the sinusoidal forcing function each point represents a separate experiment with its associated experimental error whereas all the experimental points in Fig. 6 are obtained by calculation from the response of the system to one single pulse. These variations are reflected also in the values of the process parameters (Table 3) obtained by the two methods. However, the parameters calculated assuming the lead/lag system show much closer agreement (with the exception of the dead time) than those employing the first-order lag model. The values of the damping coefficient in each case are greater than unity indicating the second-order lag constitutes an overdamped contribution.

5. CONCLUSIONS

The results of experimental and theoretical investigations concerning the dynamics of a countercurrent flow plate heat exchanger have shown that the transfer

function relating the outlet temperature of the cold stream and the mass flow of the hot stream is best represented by an overdamped second-order lag coupled with a first-order lead with dead time, namely

$$G(s) = \frac{\bar{\theta}_{co}(s)}{\bar{m}_h(s)} = \frac{H(\tau_a s + 1)\, e^{-\tau_d s}}{\tau_p^2 s^2 + 2\zeta\tau s + 1}.$$

Acknowledgements—The authors are indebted to Dr W. M. Kassim, University of Baghdad, for providing laboratory facilities and for his constant help and encouragement with the investigations. Dr J. S. Al-Jamali's efforts are also appreciated for arranging experimental facilities and for providing continuous encouragement during the course of this work.

REFERENCES

1. R. Harriott, *Process Control*. McGraw-Hill, New York (1964).
2. P. H. Cross, The use of plate heat exchanger for energy economy, *Chem. Engr* **378**, 87–90 (1982).
3. G. W. McKnight and C. W. Worley, Dynamic analysis of plate heat exchanger system, *ISA Proc.* Paper No. 53-6-1, 68–75 (1953).
4. A. Ito and M. Masubuchi, Dynamic analysis of a plate heat exchanger system, *Bull. J.S.M.E. (Japan)* **20**(142), 434–441 (1977).
5. T. Zaleski and J. Tejszerski, Dynamics of the plate heat exchangers, Chemplant '80, Comput. in the Design and Erection of Chem. Plants, V2 Heviz, Hung., Budapest, Hung. Chem. Soc., pp. 779–790, 3–5 September (1980).
6. J. M. Douglas, *Process Control*, Vol. 1, *Analysis of Dynamic Systems*. Prentice-Hall, Englewood Cliffs, New Jersey (1972).
7. A. Ito and M. Masubichi, *Technol. Rep. Osaka Univ.* **27**, 261–269 (1977).
8. A. A. McKillip and W. L. Dunkley, (Plate heat exchanger) heat transfer, Turbulence promoters and flexible plate arrangements give high heat-transfer rates at low pressure drops. *Ind. Engng Chem.* **52**, 740–744 (1960).
9. M. Ghanim, M.Sc. Thesis, University of Baghdad, Iraq (1982).
10. H. H. Rosenbrock, An automatic method for finding the greatest or least value of function, *Computer J.* **3**, 175–183 (1960).
11. A. Burns, C. P. Jefferson and A. M. Willmott, Use of lead/lag approximations in modeling thermal regenerators systems, *J. Dynamic Systems Measmt Control, Trans. ASME* **103**, 49–53 (1981).
12. G. Gilles, New results in modelling heat exchanger dynamiçs, *J. Dynamic Systems Measmt Control, Trans. ASME* **96**, 277–282 (1974).
13. L. C. W. Dixon, *Non-linear Optimisation*. English Universities Press, London (1972).

APPENDIX A

Assuming U to be constant, an unsteady-state energy balance around the cold plate gives

$$m_c C(\theta_{ci} - \theta_{co}(t)) + m_h(t) C(\theta_{hi} - \theta_{ho}(t)) = M_c C \frac{d\theta_{co}(t)}{dt} \quad \text{(A1a)}$$

$$\therefore m_c\theta_{ci} - m_c\theta_{co}(t) + m_h(t)\theta_{hi} - m_h(t)\theta_{ho}(t) = M_c \frac{d\theta_{co}(t)}{dt}. \quad \text{(A1b)}$$

Using a two variable Taylor series expansion about the unsteady-state for the non-linear term [13]

$$m_h(t)\theta_{ho}(t) = m_h\theta_{ho} + (m_h(t) - m_h)\left.\frac{\partial[m_h(t)\theta_{ho}(t)]}{\partial m_h(t)}\right|_{SS} + (\theta_{ho}(t) - \theta_{ho})\left.\frac{\partial[m_h(t)\theta_{ho}(t)]}{\partial\theta_{ho}(t)}\right|_{SS} + \text{higher order terms} \quad \text{(A2)}$$

(where SS implies calculation at the steady state).

For small perturbations about the steady state higher order terms can be neglected and equation (A2) approximates to

$$m_h(t)\theta_{ho}(t) = m_h\theta_{ho} + m_h(\theta_{ho}(t) - \theta_{ho}) + \theta_{ho}(m_h(t) - m_h). \quad \text{(A3)}$$

Substituting equation (A3) into equation (A1b) gives

$$m_c\theta_{ci} - m_c\theta_{co}(t) + m_h(t)\theta_{hi} - m_h\theta_{ho} - m_h(\theta_{ho}(t) - \theta_{ho}) - \theta_{ho}(m_h(t) - m_h) = M_c \frac{d\theta_{co}(t)}{dt}. \quad \text{(A4a)}$$

Subtracting the steady-state form of equation (A4a) from equation (A4a) and writing

$$\bar{\theta}_{co} = \theta_{co}(t) - \theta_{co}, \quad \bar{m}_h = m_h(t) - m_h, \quad \bar{\theta}_{ho} = \theta_{ho}(t) - \theta_{ho},$$

and

$$\frac{d\bar{\theta}_{co}}{dt} = \frac{d}{dt}(\theta_{co}(t) - \theta_{co})$$

$$\frac{M_c}{m_c}\frac{d\bar{\theta}_{co}}{dt} + \bar{\theta}_{co} = \frac{(\theta_{hi} - \theta_{ho})}{m_c}\bar{m}_h - \frac{m_h}{m_c}\bar{\theta}_{ho}. \quad \text{(A4b)}$$

Putting

$$\tau_c = \frac{M_c}{m_c}, \quad K_1 = \frac{\theta_{hi} - \theta_{ho}}{m_c} \quad \text{and} \quad K_2 = \frac{m_h}{m_c}$$

$$\tau_c\frac{d\bar{\theta}_{co}}{dt} + \bar{\theta}_{co} = K_1\bar{m}_h - K_2\bar{\theta}_{ho}.$$

Applying the Laplace transform

$$\tau_c s\bar{\theta}_{co}(s) + \bar{\theta}_{co}(s) = K_1\bar{m}_h(s) - K_2\bar{\theta}_{ho}(s)$$

$$\therefore \bar{\theta}_{co}(s) = \frac{K_1}{1+\tau_c s}\bar{m}_h(s) - \frac{K_2}{1+\tau_c s}\bar{\theta}_{ho}(s). \quad \text{(A5)}$$

An unsteady-state energy balance around the hot plate gives

$$m_h(t)C(\theta_{hi} - \theta_{ho}(t)) + m_c C(\theta_{ci} - \theta_{co}(t)) = M_h C\frac{d\theta_{ho}(t)}{dt}. \quad \text{(A6)}$$

This can be treated in the same manner as equation (A1a) to yield

$$\bar{\theta}_{ho}(s) = \frac{K_3}{1+\tau_h s}\bar{m}_h(s) - \frac{K_4}{1+\tau_h s}\bar{\theta}_{co}(s) \quad \text{(A7)}$$

where

$$\tau_h = \frac{M_h}{m_h}, \quad K_3 = \frac{\theta_{hi} - \theta_{ho}}{m_h} \quad \text{and} \quad K_4 = \frac{m_c}{m_h}.$$

Eliminating $\bar{\theta}_{ho}(s)$ between equations (A5) and (A7) gives

$$\frac{\bar{\theta}_{co}(s)}{\bar{m}_h(s)} = \frac{K_1\tau_h s + (K_1 - K_2K_3)}{\tau_c\tau_h s^2 + (\tau_c + \tau_h)s + (1 - K_2K_4)}.$$

But

$$1 - K_2K_4 = 1 - \frac{m_h}{m_c}\frac{m_c}{m_h} = 0$$

and

$$K_1 - K_2K_3 = \frac{\theta_{hi}-\theta_{ho}}{m_c} - \frac{m_h}{m_c}\frac{(\theta_{hi}-\theta_{ho})}{m_h} = 0$$

$$\therefore G(s) = \frac{\bar{\theta}_{co}(s)}{\bar{m}_h(s)} = \frac{K_1\tau_h}{\tau_c\tau_h s+(\tau_c+\tau_h)} = \frac{K}{1+\tau_p s} \quad \text{(A8)}$$

where

$$K = \frac{K_1\tau_h}{\tau_c+\tau_h} \quad \text{and} \quad \tau_p = \frac{\tau_c\tau_h}{\tau_c+\tau_h}.$$

APPENDIX B

For U as a function of time, i.e. $U(t)$, an unsteady-state energy balance around the cold plate gives

$$m_cC(\theta_{ci}-\theta_{co}(t))+AU(t)\left\{\frac{\theta_{hi}-\theta_{co}(t)}{2} + \frac{\theta_{ho}(t)-\theta_{ci}}{2}\right\} = M_cC\frac{d\theta_{co}(t)}{dt}. \quad \text{(B1)}$$

Substituting equation (10) and putting $A/2 = Z$

$$m_cC(\theta_{ci}-\theta_{co}(t)) + \frac{Zm_h^b(t)}{am_h^b(t)+c}(\theta_{hi}+\theta_{ho}(t)-\theta_{ci}-\theta_{co}(t)) = M_cC\frac{d\theta_{co}(t)}{dt}. \quad \text{(B2)}$$

The non-linear terms in equation (B2) are linearized using the Taylor series as in Appendix A. Hence

$$\frac{Zm_h^b(t)}{am_h^b(t)+c}\theta_{hi} = \frac{Zm_h^b\theta_{hi}}{am_h^b+c} + \frac{\theta_{hi}Zcbm_h^{b-1}}{(am_h^b+c)^2}(m_h(t)-m_h) = Q\theta_{hi}+R\theta_{hi}(m_h(t)-m_h) \quad \text{(B3)}$$

where

$$Q = \frac{Zm_h^b}{am_h^b+c} \quad \text{and} \quad R = \frac{Zcbm_h^{b-1}}{(am_h^b+c)^2}.$$

Similarly

$$\frac{Zm_h^b(t)\theta_{ci}}{am_h^b(t)+c} = Q\theta_{ci}+R\theta_{ci}(m_h(t)-m_h) \quad \text{(B4)}$$

$$\frac{Zm_h^b(t)\theta_{ho}(t)}{am_h^b(t)+c} = Q\theta_{ho}+Q(\theta_{ho}(t)-\theta_{ho})+R\theta_{ho}(m_h(t)-m_h) \quad \text{(B5)}$$

and

$$\frac{Zm_h^b(t)\theta_{co}(t)}{am_h^b(t)+c} = Q\theta_{co}+Q(\theta_{co}(t)-\theta_{co})+R\theta_{co}(m_h(t)-m_h). \quad \text{(B6)}$$

Substituting equations (B3)–(B6) into equation (B2) and subtracting the steady-state form of equation (B2) leads to

$$-m_cC(\theta_{co}(t)-\theta_{co})+R\theta_{hi}(m_h(t)-m_h)+Q(\theta_{ho}(t)-\theta_{ho}) + R\theta_{ho}(m_h(t)-m_h)-R\theta_{ci}(m_h(t)-m_h) - Q(\theta_{co}(t)-\theta_{co})-R\theta_{co}(m_h(t)-m_h) = M_cC\frac{d\theta_{co}(t)}{dt}.$$

Substituting the deviation variables (A4b) and writing

$$\tau_c = \frac{M_cC}{m_cC+Q}, \quad K_5 = \frac{Q}{m_cC+Q}, \quad K_6 = \frac{R(\theta_{hi}+\theta_{ho}-\theta_{ci}-\theta_{co})}{m_cC+Q}$$

$$\tau_c\frac{d\bar{\theta}_{co}(t)}{dt} + \bar{\theta}_{co}(t) = K_5\bar{\theta}_{ho}(t)+K_6\bar{m}_h(t).$$

Applying the Laplace transform and rearranging gives

$$\bar{\theta}_{co}(s) = \frac{K_5}{1+\tau_c s}\bar{\theta}_{ho}(s) + \frac{K_6}{1+\tau_c s}\bar{m}_h(s). \quad \text{(B7)}$$

The unsteady-state energy balance around the hot plate leads to

$$m_h(t)C(\theta_{hi}-\theta_{ho}(t))-AU(t)\left\{\frac{\theta_{hi}-\theta_{co}(t)}{2}+\frac{\theta_{ho}(t)-\theta_{ci}}{2}\right\} = M_hC\frac{d\theta_{ho}(t)}{dt}. \quad \text{(B8)}$$

This can be treated in the same manner as equation (B1) to yield

$$\bar{\theta}_{ho}(s) = \frac{K_7}{1+\tau_h s}\bar{\theta}_{co}(s) + \frac{K_8}{1+\tau_h s}\bar{m}_h(s) \quad \text{(B9)}$$

where

$$\tau_h = \frac{M_hC}{m_hC+Q}, \quad K_7 = \frac{Q}{m_hC+Q}$$

and

$$K_8 = \frac{C(\theta_{hi}-\theta_{ho})-R(\theta_{hi}+\theta_{ho}-\theta_{ci}-\theta_{co})}{m_hC+Q}.$$

Eliminating $\bar{\theta}_{ho}(s)$ between equations (B8) and (B9) leads to

$$G(s) = \frac{\bar{\theta}_{co}(s)}{\bar{m}_h(s)} = \frac{K_6\tau_h s+(K_6+K_5K_8)}{\tau_c\tau_h s^2+(\tau_c+\tau_h)s+(1-K_5K_7)} = \frac{H(\tau_a s+1)}{\tau_p^2 s^2+2\zeta\tau_p s+1} \quad \text{(B10)}$$

where

$$\tau_a = \frac{K_6\tau_h}{H(1-K_5K_7)}$$

$$\tau_p = \left\{\frac{\tau_c\tau_h}{1-K_5K_7}\right\}^{1/2}$$

and

$$\zeta = \frac{\tau_c+\tau_h}{2[\tau_c\tau_h(1-K_5K_7)]^{1/2}}.$$

CARACTERISTIQUES DYNAMIQUES D'UN ECHANGEUR DE CHALEUR A PLAQUES ET A CONTRECOURANT

Résumé—On analyse théoriquement et expérimentalement les caractéristiques dynamiques d'un échangeur de chaleur à plaques. Des modèles de premier et de second ordre avec temps mort sont proposés et testés à l'aide des résultats expérimentaux obtenus avec des tests sinusoïdaux et pulsés. On trouve que la réponse dynamique de la température de sortie θ_{co} du courant froid vis-à-vis du débit masse m_h du courant chaud est plus proche de la fonction de transfert du second ordre

$$\frac{\bar{\theta}_{co}(s)}{\bar{m}_h(s)} = \frac{H(\tau_a s+1)e^{-\tau_d s}}{\tau_p^2 s^2+2\zeta\tau_p s+1}.$$

DAS DYNAMISCHE VERHALTEN EINES GEGENSTROM-PLATTENWÄRMEAUSTAUSCHERS

Zusammenfassung—Das dynamische Verhalten eines Plattenwärmeaustauschers wurde theoretisch und experimentell untersucht. Modelle erster und zweiter Ordnung mit Totzeit werden vorgeschlagen und mit Meßergebnissen bei sinus- und pulsförmiger Erregung verglichen. Es zeigt sich, daß das dynamische Verhalten der Austrittstemperatur θ_{co} des kalten Stroms bei Änderung des Massenstroms m_h des heißen Stroms mit der folgenden Übertragungsfunktion zweiter Ordnung angenähert werden kann:

$$\frac{\bar{\theta}_{co}(s)}{\bar{m}_h(s)} = \frac{H(\tau_a s + 1)\,e^{-\tau_d s}}{\tau_p^2 s^2 + 2\xi\tau_p s + 1}.$$

ДИНАМИЧЕСКИЕ ХАРАКТЕРИСТИКИ ПРОТИВОТОЧНОГО ПЛАСТИНЧАТОГО ТЕПЛООБМЕННИКА

Аннотация—Проведен теоретический и экспериментальный анализ динамических характеристик пластинчатого теплообменника. Модели первого и второго порядка со временем запаздывания предложены и подтверждены результатами экспериментальной синусоидальной и импульсной проверки. Найдено, что динамический отклик температуры холодного потока на выходе θ_{co} на изменение массового потока m_h горячего течения приближается к функции переноса второго порядка

$$\frac{\bar{\theta}_{co}(s)}{\bar{m}_h(s)} = \frac{H(\tau_a s + 1)\,e^{-\tau_d s}}{\tau_p^2 s^2 + 2\zeta\tau_p s + 1}.$$